Climatological Diurnal Cycles in Clear-Sky Brightness Temperatures from the High-Resolution Infrared Radiation Sounder (HIRS)

Climatological Diurnal Cycles in Clear-Sky Brightness Temperatures from the High-Resolution Infrared Radiation Sounder (HIRS)

ANDERS V. LINDFORS

School of GeoSciences, The University of Edinburgh, Edinburgh, United Kingdom, and Climate Change Research, Finnish Meteorological Institute, Helsinki, Finland

IAN A. MACKENZIE AND SIMON F. B. TETT

School of GeoSciences, The University of Edinburgh, Edinburgh, United Kingdom

LEI SHI

National Climatic Data Center, National Oceanic and Atmospheric Administration, Asheville, North Carolina

(Manuscript received 20 May 2011, in final form 11 July 2011)

ABSTRACT

A climatology of the diurnal cycles of HIRS clear-sky brightness temperatures was developed based on measurements over the period 2002–07. This was done by fitting a Fourier series to monthly gridded brightness temperatures of HIRS channels 1–12. The results show a strong land–sea contrast with stronger diurnal cycles over land, and extending from the surface up to HIRS channel 6 or 5, with regional maxima over the subtropics. Over seas, the diurnal cycles are generally small and therefore challenging to detect. A Monte Carlo uncertainty analysis showed that more robust results are reached by aggregating the data zonally before applying the fit. The zonal fits indicate that small diurnal cycles do exist over sea. The results imply that for a long-lived satellite such as *NOAA-14*, drift in the overpass time can cause a diurnal sampling bias of more than 5 K for channel 8 (surface and lower troposphere).

1. Introduction

The High-Resolution Infrared Radiation Sounder (HIRS) instruments on board National Oceanic and Atmospheric Administration (NOAA) polar-orbiting satellites have sampled the earth's atmosphere and surface since late 1978. HIRS is a cross-track scanning radiometer that measures brightness temperatures (radiances) in 19 infrared channels, with one additional channel in the visible. It was originally developed for weather forecasting, providing information on atmospheric temperature and humidity (e.g., Hillger and Vonder Haar 1981; Schlatter 1981; Turner and Ellrott 1992), but has in more recent years also been used in climate studies (e.g., Bates and Jackson 2001; Soden et al. 2002, 2005).

The HIRS data record to date includes measurements from 13 satellite platforms, from the Television and Infrared Observation Satellite N (TIROS-N) to the *Meteorological Operational satellite A (MetOp-A)*, covering a period of more than 30 years. As with many long-term observing systems, the HIRS record features characteristics that influence its homogeneity. These are connected to, for example, intersatellite calibration, changes and uncertainties in the spectral response functions of the channels, and drift in the satellite orbits causing a systematic change in the overpass time. Although efforts have been made to examine and correct for these issues (Bates et al. 1996; Cao et al. 2005; Wang et al. 2007; Shi et al. 2008; Cao et al. 2009), there are still areas that need further attention.

We address one such area by examining the diurnal behavior of the clear-sky brightness temperatures. Knowing the characteristics of the diurnal behavior enables correcting diurnal sampling biases caused both by drifting satellite orbits and by the fact that satellite platforms have different overpass times. Previous studies

Corresponding author address: Anders Lindfors, The University of Edinburgh, School of GeoSciences, West Mains Road, Edinburgh EH9 3JW, United Kingdom.
E-mail: anders.lindfors@ed.ac.uk

DOI: 10.1175/JTECH-D-11-00093.1

have corrected for these diurnal sampling biases using climate models, as described by Jackson and Soden (2007) for HIRS. Here, we take a different approach by basing our analysis exclusively on HIRS observations. We examine the early 2000s, a period that is particularly well covered by HIRS observations and hence allows us to infer the full diurnal cycles from the satellite observations themselves. The output of the study is a climatology of the diurnal behavior of HIRS brightness temperatures.

2. HIRS data

The HIRS data and the different channels are described more in detail elsewhere (Robel 2009; Shi et al. 2008). Briefly, channels 1–7 measure in the 15-μm carbon dioxide band, providing information on the vertical temperature profile from the stratosphere (ch. 1) to the lower troposphere (ch. 7). Channel 8 is a window channel, sensing the surface and the lower atmosphere, while channel 9 is in the ozone band. Channels 10–12 are water vapor channels from near the surface (ch. 10) to the upper troposphere (ch. 12). We emphasize that each channel responds to a rather broad layer of the atmosphere according to its vertical weighting function (e.g., Fig. 2 of Jackson and Soden 2007). In this study, we concentrate on channels 1–12 because channels 13–19, located around 4 μm, and channel 20 in the visible spectrum, are influenced by solar radiation.

We use a recently developed, intersatellite-calibrated version of clear-sky, limb-corrected HIRS data. To remove cloudy pixels, we applied the cloud screening of Jackson et al. (2003), which considers both spatial and temporal variations in the brightness temperature and applies thresholds to these variations to detect clouds. Intersatellite differences were then determined based on simultaneous nadir overpass (SNO) observations (Shi et al. 2008). The SNOs are measurements taken at orbital intersections of each pair of satellites viewing the same earth target within a few seconds. They are available only at high latitudes. Analyses of the SNO data showed that the intersatellite differences vary with observed brightness temperatures. Although the SNOs span a large range of brightness temperatures, they do not cover the high temperatures typically observed in tropical regions.

Intersatellite differences at higher brightness temperatures were estimated over an equatorial ocean surface region within 20°S–20°N and 160°–100°W where diurnal variation and thus temporal sampling biases, as confirmed by climate model simulations, are at minimum. Differences in regional monthly mean values were obtained for overlapping satellites. By combining these low-latitude data with those from SNOs, we constructed temperature-dependent intersatellite differences covering the whole range of observed brightness temperatures. This information was used for correcting the brightness temperatures of all HIRS instruments to the level of *NOAA-12*.

Our analysis concentrates on the period 2002–07. For this period, intersatellite corrected data are available from *NOAA-14* (years 2002–05), *NOAA-15* (2002–07), *NOAA-16* (2002–04), and *NOAA-17* (2002–07). This means that, at best, there are eight overpasses available for a certain location and a given day, thus giving a good coverage of the diurnal behavior of the measured brightness temperatures. The fact that some of the satellites, in particular *NOAA-14* and *NOAA-15*, drifted in their local overpass time further improves the diurnal sampling.

To analyze the diurnal cycle of the brightness temperatures, the HIRS data were gridded onto a monthly 2.5° × 2.5° latitude–longitude grid. Thus, the gridded data of July, for example, include data from all July months over the period 2002–07. To minimize the uncertainty introduced by the limb correction, only near-nadir observations (scan positions 26–31; following Jackson and Soden 2007) were included. As a minimum requirement on data availability, only grid boxes with at least 10 observations in each quarter of the 24-h day were included in the analysis.

3. Fits to diurnal cycles

To facilitate a description of the diurnal behavior of the HIRS brightness temperatures, a second-order Fourier series (similar to Lee et al. 2007; Mears et al. 2003) was fitted to the data of each month, grid box, and channel:

$$T_b = a_0 + a_1 \cos\frac{\pi(t - t_1)}{12} + a_2 \cos\frac{2\pi(t - t_2)}{12}. \qquad (1)$$

Here, T_b is the brightness temperature, t is the local time (in hours), and a_0–a_2 and t_1–t_2 are the fit parameters. Note that a_0 represents the mean level of T_b, a_1 is half the peak-to-peak amplitude of the 24-hourly oscillation (the first harmonic), and a_2 is half the peak-to-peak amplitude of the 12-hourly oscillation (the second harmonic)—higher harmonics tend to be very small and were therefore disregarded—and t_1 and t_2 are the phases of the two harmonics. These parameters define the diurnal behavior of the HIRS brightness temperatures, as approximated by Eq. (1). The fits were determined using least squares regression.

It is noteworthy that the a_1 component (24-hourly frequency) essentially cancels out between the ascending and descending node observations of a sun-synchronous polar-orbiting satellite because they are taken approximately 12 h (one-half of a period) apart. Thus, it is the a_2

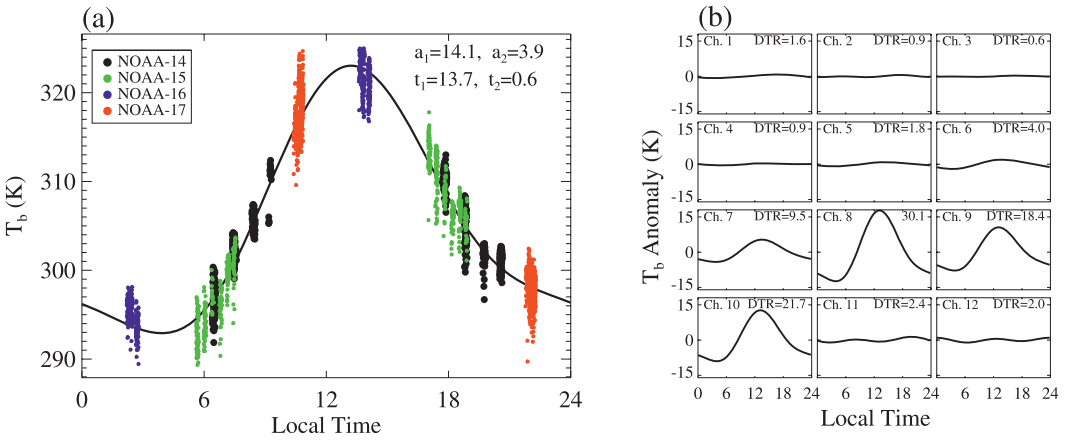

FIG. 1. (a) HIRS channel 8 brightness temperatures (T_b) for July and a 2.5° × 2.5° grid box centered on 31.25°N, 1.25°E together with the Fourier series fitted to the data. The numbers indicate the values of the fit parameters (a_1, a_2, t_1, and t_2). (b) The fits of the individual channels, plotted as T_b anomalies, for the same grid box. The numbers show the diurnal brightness temperature range.

component that is largely responsible for the diurnal sampling biases. This means also that the intersatellite correction discussed above, which is based on both ascending and descending passes, will include only a small contribution from the a_1 component.

Figure 1a shows, as an example, the gridded HIRS brightness temperatures of July and channel 8 together with the Fourier fit for a grid box over the Saharan Desert in northern Africa. Because channel 8 is a surface channel, the diurnal variation of the brightness temperature is rather strong, as expected in this dry, subtropical region. The figure also shows the extra coverage over the 24-h day gained thanks to the drifting satellite orbits. The ascending node observation of *NOAA-15*, for example, gradually drifts toward local noon from 1845 local time (LT) in 2002 to around 1700 LT in 2007. For *NOAA-14* the span is even larger.

The brightness temperatures within each grid box include both year-to-year and day-to-day variability. Yearly groups of similar local time can, for example, be seen for the drifting satellites, *NOAA-14* and *NOAA-15*, in Fig. 1a. Our assumption is that by aggregating the data over 6 years (2002–07), these variations are largely averaged out, and hence the fit parameters are representative of the climatological diurnal behavior of the HIRS brightness temperatures.

4. Results

We present the results of our study by examining (i) the fit parameters a_1 and a_2 and (ii) the diurnal brightness temperature range (DTR), defined as the difference between the maximum and the minimum of the fitted function [Eq. (1)].

Figure 1b shows the Fourier-fitted brightness temperatures of each HIRS channel as anomalies from the daily mean for July and the Saharan grid box. The diurnal cycle weakens when moving from the surface (ch. 8) to higher layers of the atmosphere (ch. 7–1). The DTR of channel 8 is 30.1 K, decreasing to 4.0 K for channel 6 and staying below 1 K for channels 4–2. Channels 1 and 5, and the water vapor channels 11 and 12, have DTRs between 1.5 and 2.5 K, while both channels 9 and 10, which include a considerable contribution from the surface, exhibit a strong diurnal cycle.

Figure 2 shows the January and July global distribution of a_1 and a_2 of channel 8. The strongest diurnal cycles (largest a_1 and a_2) prevail over the summer hemisphere subtropical land areas and mountainous regions in the middle latitudes. The diurnal cycle has a minimum over the intertropical convergence zone. In this region, for example over the northern parts of South America and equatorial Africa, convective cloudiness developing during the day tends to suppress the maximum temperature. For a similar reason, the region over India has larger a_1 and a_2 during January than during the monsoon season in July. A seasonal variation can be seen in the Northern Hemisphere midlatitudes particularly in a_1, for example, over Siberia.

There is a strong land–sea contrast in the diurnal behavior of channel 8 brightness temperatures (Fig. 2). Both a_1 and a_2 are mostly below 1 K over seas. We note, however, that these values should be interpreted with caution as it is challenging to detect small diurnal cycles in the HIRS brightness temperatures because of underlying natural variability and limited sampling.

To estimate the uncertainty of the derived fit parameters, we used a Monte Carlo approach. Measured

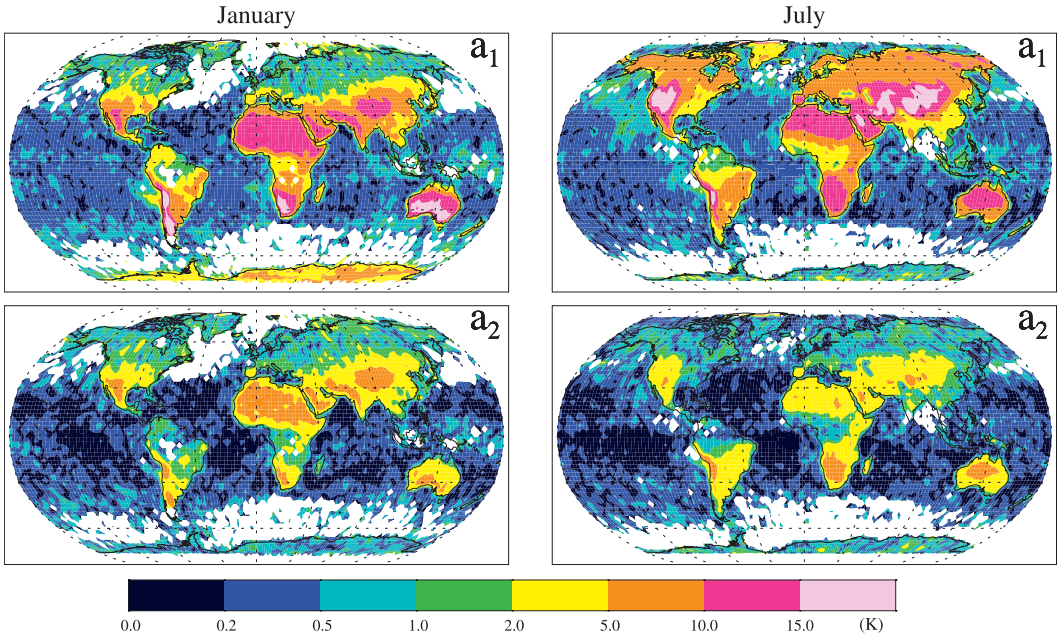

FIG. 2. The fit parameters (top) a_1 and (bottom) a_2 of HIRS channel 8 of (left) January and (right) July. White indicates regions where the minimum requirement on data availability is not met.

brightness temperatures within each grid box were replaced with random numbers from a normal distribution with the same mean value and standard deviation as the observations. Here, we used the pooled standard deviation of the observations grouped according to satellite and ascending or descending node, which excludes any systematic differences between the groups arising from, say, the diurnal behavior. This approach preserves the observation times and the number of observations within each grid box but does not account for possible intersatellite biases.

The Monte Carlo analysis shows that when the true diurnal cycle is flat (both a_1 and a_2 are zero), the estimates of a_1 and a_2 are biased toward small positive numbers. This follows from them having a one-sided distribution, always being zero or positive. We ran 300 iterations for each grid box. The results show that the uncertainty is dominated by the number of observations and the natural variability in each grid box. For channel 8, the 95th percentile of both a_1 and a_2 is typically 0.2 K over most of the tropical and subtropical oceans, and increases toward the poles, with values of around 1 K over the summer hemisphere high latitudes and up to 2 K and above for the cloudy and poorly sampled winter hemisphere high latitudes. This means that the a_2 values over the oceans in Fig. 2 are, in fact, largely consistent with zero, whereas a_1 implies that a diurnal cycle does exist over large parts of the oceans.

To improve the sampling and reduce the uncertainty, we performed a zonal analysis, separately for sea and land, aggregating all observations from each latitude band prior to fitting the Fourier series [Eq. (1)]. Coastal regions of mixed surface type were excluded from this analysis by calculating the fraction of land in each 2.5° × 2.5° grid box using a 1-km resolution land mask. Only those grid boxes with no land or more than two-thirds land were included in the zonal aggregates for sea and land, respectively. Figure 3 shows the results of the zonal analysis. The HIRS channels on the y axis of the figure represent the temperature profile (ch. 1–8), ozone (ch. 9), and water vapor (ch. 10–12), as discussed above. According to a Monte Carlo analysis analogous to the one discussed above, the 95th percentile of a_1 and a_2 of this zonal analysis is predominantly less than 0.2 K, hence the choice of white for the values 0–0.2 K in the figure.

Over land (Fig. 3, left column), the zonal fit parameters of July show, consistent with the situation over the Saharan grid box (Fig. 1b), that the diurnal cycles of the HIRS brightness temperatures are strongest near the surface (ch. 8) as well as in the ozone channel (ch. 9) and the near-surface water vapor channel (ch. 10). Both a_1 and a_2 decrease with height, and although a_1 generally dominates over a_2, parameter a_2 also shows magnitudes exceeding 0.5 K for channels 6–10, typically, in the subtropics.

Over seas (Fig. 3, right column), the diurnal cycles are small. In particular, a_2 is predominantly less than 0.2 K. The value of a_1, on the other hand, indicates that a small diurnal cycle does exist, which cannot be explained by

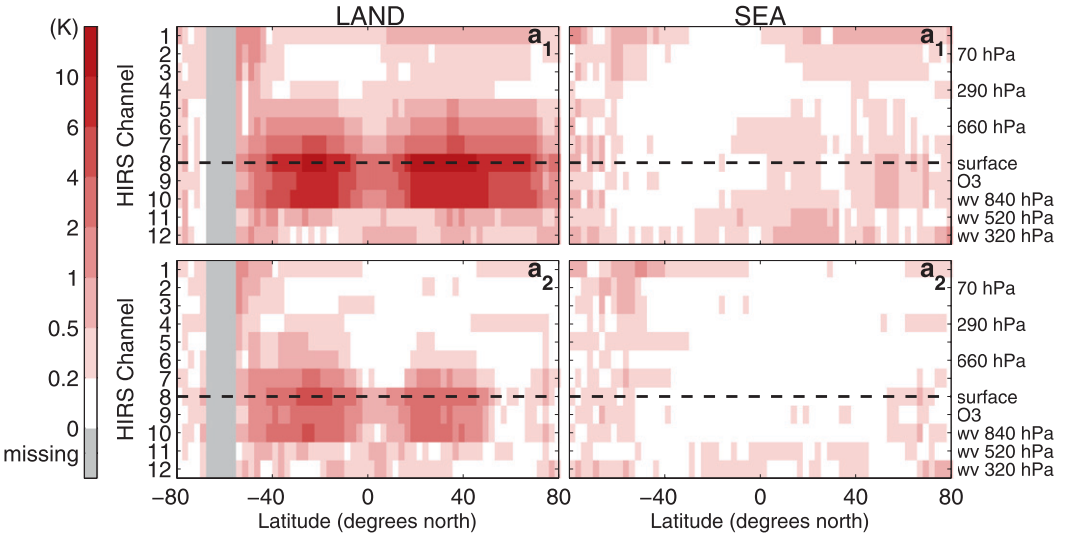

FIG. 3. Zonal fit parameters (top) a_1 and (bottom) a_2 of July for (left) land and (right) sea. The secondary y axis illustrates which part of the atmosphere the channels are most sensitive to assuming a tropical atmospheric profile (wv stands for water vapor and O3 for ozone). The dashed line represents the surface.

sampling uncertainties. In the Northern Hemisphere, for example, a_1 of channel 8 takes values between 0.2 and 1 K, mostly resulting in DTRs of 0.3–1.5 K for July. Given that HIRS channel 8 responds not only to the surface but also to the lower part of the atmosphere, which is expected to warm more than the sea surface over the course of the day, these results are consistent with, for example, Kawai and Wada (2007). They showed, using microwave satellite measurements, day–night differences in the sea surface temperature of ~0.2–l K for June–August in the Northern Hemisphere.

Interestingly, channel 1 (stratosphere) shows an a_1 value exceeding 0.5 K for much of the Northern Hemisphere in July. A similar diurnal cycle was revealed by radio occultation data over the tropics, at an altitude of 30 km (Zeng et al. 2008). The water vapor channels 11 and 12 show a weak diurnal cycle (both a_1 and a_2) over both land and sea. In addition, a_1 of channel 12 exhibits a weak but distinguishable maximum in the northern tropical latitudes, indicating a stronger diurnal cycle in the atmospheric water vapor corresponding to the intertropical convergence zone. This is consistent with a regional analysis using geostationary satellite data from the Spinning Enhanced Visible and Infrared Imager (SEVIRI) instrument (Chung et al. 2007). Over the course of the year (not shown), this weak maximum follows the sun.

Taken as a whole, our results are in general agreement with the analysis of Seidel et al. (2005), who used radiosonde data to estimate the diurnal temperature cycle. They found, like us, a strong land–sea contrast with stronger diurnal cycles over land, and extending from the surface up to 850 hPa. However, their surface amplitudes, ranging from 1 to 4 K, are substantially smaller than ours. This difference arises partly because the satellite data include a contribution from the surface skin, which is not measured by the sondes, and partly because the radiosonde data are limited in their geographical coverage (e.g., not covering dry subtropical regions to any great extent).

5. Implications for diurnal sampling biases

To examine the implications of our results, we computed the correction required to convert the observed brightness temperatures to a nominal noon local time. We did this using the zonal land and sea values of a_1, a_2, t_1, and t_2 [Eq. (1)] for each month together with information on the evolution of the satellite orbits. We then area weighted the outcome to obtain a global average. Figure 4 shows, for *NOAA-14*, the maximum diurnal sampling bias, defined as the difference between the largest and the smallest correction with respect to local noon. The maximum sampling biases are largest for channels 7–11, exceeding 5 K for channel 8. The sampling bias of all channels is of considerable magnitude compared to an expected climate trend of 0.1–0.2 K decade^{-1}. For many channels, however, and particularly over ocean, the diurnal sampling bias is small compared to intersatellite and limb corrections. We also found that the maximum diurnal sampling bias exhibits a seasonal cycle with maxima at the equinoxes.

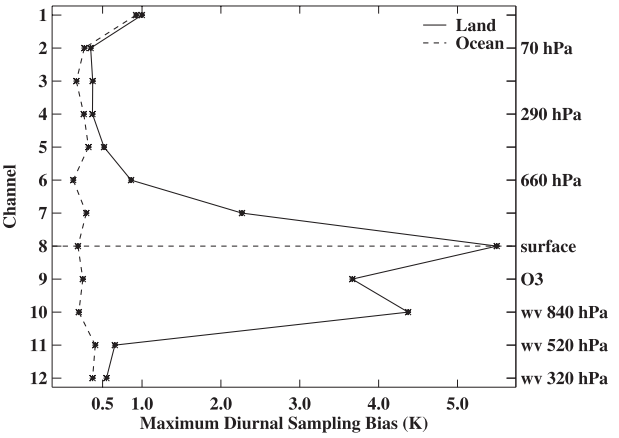

FIG. 4. Maximum diurnal sampling bias of *NOAA-14*. The secondary *y* axis and the horizontal dashed line are as in Fig. 3. See text for discussion on uncertainty.

Furthermore, we used the Monte Carlo results to estimate the uncertainty in the diurnal sampling biases presented in Fig. 4. Being conservative, we assumed that all meridional uncertainties covary and then tested three assumptions on the covariance of the zonal fit parameters (a_1, a_2, t_1, t_2): (i) all parameters covary, (ii) no covariance between the parameters, and (iii) anticorrelation between t_1 and t_2, on one hand, and a_1 and a_2, on the other. For each assumption, the standard errors on the diurnal sampling bias were small at about 2% of the actual values over land and less than 10% over sea. This is because the low and midlatitudes, which cover a large area of the globe, are well sampled and thus have only a small uncertainty according to our Monte Carlo analysis (95th percentiles of a_1 and a_2 mainly at 0.1 K or below).

6. Discussion

A climatology of the diurnal cycles of HIRS brightness temperatures was developed based on HIRS satellite measurements over the period 2002–07. Although this period is short from a climatological perspective, our use of zonally aggregated data and the absence of interannual variability in insolation, the main driver of the diurnal cycle, lends confidence that our results are representative. Other sources of uncertainty not accounted for in our Monte Carlo error analysis relate to the quality and homogeneity of the multi-instrument dataset used.

As we only characterized clear-sky data, our analysis represents the typical diurnal behavior of HIRS clear-sky brightness temperatures, rather than an overall climatology. This climatology of Fourier-fitted diurnal cycles of the HIRS clear-sky brightness temperatures will be useful for correcting the long-term HIRS data record, extending more than 30 years into the past, for diurnal sampling biases. The results can also serve as a basis for testing climate models and for more detailed studies on the diurnal behavior of the HIRS brightness temperatures.

The climatology is available upon request.

Acknowledgments. We thank the National Centre for Earth Observation for funding (NERC Grant NE/F001436/1). AVL was partly funded by the Academy of Finland, decision 133259. Hai-Tien Lee is acknowledged for providing local equator crossing times and Viju John for sharing initial codes. We made use of resources of the Edinburgh Compute and Data Facility Eddie. We thank the anonymous reviewers for their useful comments.

REFERENCES

Bates, J. J., and D. L. Jackson, 2001: Trends in upper-tropospheric humidity. *Geophys. Res. Lett.,* **28,** 1695–1698.

——, X. Wu, and D. L. Jackson, 1996: Interannual variability of upper-troposphere water vapor band brightness temperature. *J. Climate,* **9,** 427–438.

Cao, C., H. Xu, J. Sullivan, L. McMillin, P. Ciren, and Y. Hou, 2005: Intersatellite radiance biases for the High-Resolution Infrared Radiation Sounders (HIRS) on board *NOAA-15,-16,* and *-17* from simultaneous nadir observations. *J. Atmos. Oceanic Technol.,* **22,** 381–395.

——, M. Goldberg, and L. Wang, 2009: Spectral bias estimation of historical HIRS using IASI observations for improved fundamental climate data records. *J. Atmos. Oceanic Technol.,* **26,** 1378–1387.

Chung, E. S., B. J. Sohn, J. Schmetz, and M. Koenig, 2007: Diurnal variation of upper tropospheric humidity and its relations to convective activities over tropical Africa. *Atmos. Chem. Phys.,* **7,** 2489–2502.

Hillger, D. W., and T. H. Vonder Haar, 1981: Retrieval and use of high-resolution moisture and stability fields from *Nimbus 6* HIRS radiances in pre-convective situations. *Mon. Wea. Rev.,* **109,** 1788–1806.

Jackson, D. L., and B. J. Soden, 2007: Detection and correction of diurnal sampling bias in HIRS/2 brightness temperatures. *J. Atmos. Oceanic Technol.,* **24,** 1425–1438.

——, D. P. Wylie, and J. J. Bates, 2003: The HIRS Pathfinder Radiance Data Set (1979–2001). Preprints, *12th Conf. on Satellite Meteorology and Oceanography,* Long Beach, CA, Amer. Meteor. Soc., P1.8. [Available online at http://ams.confex.com/ams/pdfpapers/57094.pdf.]

Kawai, Y., and A. Wada, 2007: Diurnal sea surface temperature variation and its impact on the atmosphere and ocean: A review. *J. Oceanogr.,* **63,** 721–744.

Lee, H., A. Gruber, R. G. Ellingson, and I. Laszlo, 2007: Development of the HIRS outgoing longwave radiation climate dataset. *J. Atmos. Oceanic Technol.,* **24,** 2029–2047.

Mears, C., M. Schabel, and F. Wentz, 2003: A reanalysis of the MSU channel 2 tropospheric temperature record. *J. Climate,* **16,** 3650–3664.

Robel, J., cited 2009: NOAA KLM User's Guide. NOAA, National Climatic Data Center. [Available online at http://www.ncdc.noaa.gov/oa/pod-guide/ncdc/docs/klm/cover.htm.]

Schlatter, T. W., 1981: An assessment of operational TIROS-N temperature retrievals over the United States. *Mon. Wea. Rev.,* **109,** 110–119.

Seidel, D., M. Free, and J. Wang, 2005: Diurnal cycle of upper-air temperature estimated from radiosondes. *J. Geophys. Res.,* **110,** D09102, doi:10.1029/2004JD005526.

Shi, L., J. J. Bates, and C. Cao, 2008: Scene radiance–dependent intersatellite biases of HIRS longwave channels. *J. Atmos. Oceanic Technol.,* **25,** 2219–2229.

Soden, B. J., R. T. Wetherald, G. L. Stenchikov, and A. Robock, 2002: Global cooling after the eruption of Mount Pinatubo: A test of climate feedback by water vapor. *Science,* **296,** 727–730.

——, D. L. Jackson, V. Ramaswamy, M. D. Schwarzkopf, and X. Huang, 2005: The radiative signature of upper tropospheric moistening. *Science,* **310,** 841–844.

Turner, J., and H. Ellrott, 1992: High-latitude moisture structure determined from HIRS water vapour imagery. *Int. J. Remote Sens.,* **13,** 81–95.

Wang, L., C. Cao, and P. Ciren, 2007: Assessing *NOAA-16* HIRS radiance accuracy using simultaneous nadir overpass observations from AIRS. *J. Atmos. Oceanic Technol.,* **24,** 1546–1561.

Zeng, Z., W. Randel, S. Sokolovskiy, C. Deser, Y.-H. Kuo, M. Hagan, J. Du, and W. Ward, 2008: Detection of migrating diurnal tide in the tropical upper troposphere and lower stratosphere using the Challenging Minisatellite Payload radio occultation data. *J. Geophys. Res.,* **113,** D03102, doi:10.1029/2007JD008725.